Quantification of multiple simultaneously occurring nitrogen flows in the euphotic ocean

Min Nina Xu[1], Yanhua Wu[2], Li Wei Zheng[1], Zhenzhen Zheng[1], Huade Zhao[3], Edward A Laws[4], Shuh-Ji Kao[1]*

[1]State Key Laboratory of Marine Environmental Science, Xiamen University, Xiamen, China

[2]Shenzhen Marine Environment Monitoring Center Station, Shenzhen, China

[3]National Marine Environmental Monitoring Center, Dalian, China

[4]School of the Coast & Environment, Louisiana State University, USA

Correspondence to: Shuh-Ji Kao (sjkao@xmu.edu.cn)

Abstract

The general features of the N cycle in the sunlit ocean have been recognized, but quantitative information about multiple transformation rates among nitrogen pools, i.e., ammonium (NH_4^+), nitrite (NO_2^-), nitrate (NO_3^-) and particulate/dissolved organic nitrogen (PN/DON), are insufficient due to methodological difficulties. Recent advances in analytical methods for isotopic composition of oft-measured nitrogen species allowed us to establish a convenient isotope labelling method to quantify *in situ* dynamic nitrogen flows for euphotic water. By adding a single ^{15}N-labelled NH_4^+ tracer, we monitored the changes in concentration and isotopic composition of the total dissolved nitrogen (TDN), PN, NH_4^+, NO_2^-, and NO_3^- pools to trace the ^{15}N and ^{14}N flows. Based on mass and isotope conservations of every individual pool as well as the whole system, we formulated matrix equations with unique solution to simultaneously derive multiple nitrogen transformation rates, such as rates of NH_4^+, NO_2^-, and NO_3^- uptake; ammonia oxidation; nitrite oxidation; DON release and NH_4^+ uptake by bacteria. This isotope matrix method was designed specifically for euphotic water column incubation under simulated *in situ* condition. With consideration of multi-flows among pools, we minimized potential biases caused by non−targeted processes in traditional source-product method. The proposed isotope matrix method is convenient in terms of on-deck incubation and post-hoc data analysis and is feasible to probe effects of environmental factors (e.g., pH, temperature and light) on multiple processes under manipulated conditions.

Keywords

Ammonium oxidation, isotope, new production, nitrification, regenerated production

1. Introduction

Nitrogen (N), which is an essential element in organisms' metabolic processes, regulates productivity in the surface waters of many parts of the ocean (Falkowski, 1997; Zehr and Kudela, 2011; Casciotti, 2016). As a limiting nutrient in the euphotic zone, nitrogen rapidly interconverts among five major N compartments: particulate organic nitrogen (PN), dissolved organic nitrogen (DON), ammonium (NH_4^+), nitrite (NO_2^-), and nitrate (NO_3^-) (Fig. 1). Quantitative information on transformation rates in the marine N-cycle may advance our understanding of the coupling of autotrophic and heterotrophic processes involving carbon and nitrogen as well as the efficiency of the biological pump. Such information would also facilitate evaluation of ecosystem functions. However, the dynamic nature and complexity of the reactions involving nitrogen make it a difficult task to resolve the rates of multiple simultaneous nitrogen transformations. Inventory and isotope tracer methods have often been used to measure rate of specific process in previous studies (Ward, 2008, 2011; Lipschultz, 2008 and references therein).

The inventory method (monitoring the change of substrate and/or product concentrations over time) was often used to determine the uptake rates of ammonium, nitrite, nitrate, and urea (McCarthy and Eppley, 1972; Harvey and Caperon, 1976; Harrison and Davis, 1977; Howard et al., 2007) and to examine the occurrence and rate of nitrification (Wada and Hatton, 1971; Pakulski et al., 1995; Ward, 2011). However, unwanted processes may bias the result. For example, the substrate (ammonium) pool

57 is controlled simultaneously by consumptions via phytoplankton (PN as the product),
58 nitrifier (nitrite/nitrate as the product) and bacteria (operationally defined DON as
59 product) and by additions via remineralization from heterotrophic bacterial metabolism,
60 zooplankton excretion, and viral lysis. Similarly, the product (NO_x^-) pool of
61 nitrification is consumed contemporarily by phytoplankton during incubation.

62 The ^{15}N-labeled tracer technique has been widely used as a direct measure for
63 specific nitrogen processes since the emergence of isotope ratio mass spectrometry
64 (IRMS). For example, the addition of ^{15}N-labeled nitrate has been applied to estimate
65 new production (Dugdale and Goering, 1967; Chen, 2005; Painter et al., 2014).
66 Likewise, by incubating water to which $^{15}NH_4^+$ has been added, nitrification rate
67 ($^{15}NO_3^-$ as product; e.g. Newell et al., 2013; Hsiao et al., 2014; Peng et al., 2016) and
68 ammonium uptake rate ($^{15}N_{PN}$ as product; e.g. Dugdale and Goering, 1967; Dugdale
69 and Wilkerson, 1986; Bronk et al., 1994, 2014) can be measured, respectively, with
70 dark and light incubation. However, isotope labelling encounters similar bias problem
71 in the inventory method, i.e., multiple processes occur simultaneously involving either
72 source or product terms in the incubation bottle. In fact, these transformations among
73 pools have significant implications in biogeochemical cycle. For instance, Yool et al.
74 (2007) synthesized available global data and indicated that the fractional contribution
75 of nitrate derived from nitrification to nitrate uptake can be as high as 19–33% in the
76 euphotic zone. However, nitrate uptake rates were determined under light conditions,
77 and nitrification was determined under dark conditions (e.g. Grundle et al., 2013),

78 which are not comparable in terms of their effects on these processes. To overcome this
79 problem, 24-h incubations have been used to compensate for the diel cycle of
80 light-sensitive processes (Beman et al., 2012). Yet, 24-h incubations may cause
81 calculation artifacts due to the interference from significant transfers of ^{15}N and ^{14}N
82 among pools. A new method is needed to reconcile the above-mentioned biases and
83 the uncomparable parallel incubations.

84 Marchant et al. (2016) have reviewed recent method advances in marine N-cycle
85 studies using ^{15}N-labeling substrates combined with nanoSIMS, FISH, or HISH. These
86 methods provide qualitative information for N transfers at cellular and molecular level
87 but no quantitative rates at community level. A comprehensive review of oft-used
88 models for rate derivation was conducted by Elskens et al. (2005), who concluded that
89 oversimplified models would risk bias when their underlying assumptions are violated;
90 nevertheless, overly complex models could misinterpret part of the random noise as
91 relevant processes. Therefore, a model selection procedure was subsequently proposed
92 (De Brauwere et al., 2005). More recently, Pfister et al. (2016) applied isotope tracer
93 technique and mass conservation model onto tidal ponds study to explore nitrogen
94 flows among dissolved nitrogen pools (NH_4^+, NO_2^- and NO_3^-) and found that benthic
95 macrobiota plays important role in regulating remineralization flow. They also proved
96 that the dilution effect significantly biased the results obtained by source-product
97 models. Nevertheless, for the euphotic zone where competing processes co-occur, an

innovative and convenient method for on-deck incubation to measure *in situ* multiple N flows is needful.

In this study, we propose an "isotope matrix method". To avoid perturbations, the concentration of the tracer was limited to < 10% or 20 % of the substrate concentration, as suggested by previous researchers (Raimbault and Garcia, 2008; Middelburg and Nieuwenhuize, 2000; Painter et al., 2014). One single tracer, $^{15}NH_4^+$, was added into incubation bottle to trace the ^{15}N flow among the nitrogen pools under simulated *in situ* conditions. Almost all the most fundamental processes in the N cycle can be quantified with this newly proposed method. To demonstrate the applicability of the method, we conducted incubation experiments for low-nutrient water in the western North Pacific and for high-nutrient coastal water off southeastern China coast. Thank for recent advances in these analytical methods for concentration and isotopic composition of various nitrogen species, this isotope matrix method becomes applicable to quantify *in situ* dynamic nitrogen flows for euphotic water.

2. Isotope matrix method

2.1 Framework of the inter-connections among nitrogen pools

In the oxygenated and well-lit euphotic zone, the transformations of N among NH_4^+, NO_2^-, NO_3^-, PN, and DON are shown in Fig. 1. The PN is operationally defined as the particulate organic nitrogen trapped on a GF/F filter (> 0.7μm). Dissolved inorganic nitrogen (DIN) and DON are the inorganic and organic nitrogen, respectively, in the dissolved fraction that passes through a polycarbonate membrane with a 0.22 μm

119 pore size. Since DON includes the N in numerous dissolved organic N compounds,
120 including unidentified organics, urea, amino acids, amines, and amides, DON
121 represents the "bulk" DON and is calculated by subtracting the concentrations of NH_4^+,
122 NO_2^-, and NO_3^- (DIN) from the total dissolved N (TDN).

123 We consider two different types of schemes in our method: low nitrogen and high
124 nitrogen (Fig. 1a and 1b). The low nutrient scheme is for the open ocean. The high
125 nutrient scheme is for estuary and coastal environments where three dissolved
126 inorganic nitrogen species co-exist. Below, we describe the rationale of model
127 structures for the two cases.

128 The consumption of reactive inorganic nitrogen (NH_4^+, NO_2^-, and NO_3^-) is
129 dominated by photosynthetic uptake by phytoplankton (F1 and F4 in Fig. 1a; F1, F3,
130 and F5 in Fig. 1b). Heterotrophic bacteria may also be important actors for NH_4^+
131 assimilation (Laws, 1985), and was confirmed by studies later on (e.g. Middelburg and
132 Nieuwenhuize, 2000; Veuger et al., 2004). We took it into account as well (F6 in Fig.
133 1a and F8 in Fig. 1b) to explore its importance. Though NO_2^- may be released during
134 NO_3^- uptake (Lomas and Lipschultz, 2006), little NO_2^- production from NO_3^- was
135 detected (Santoro et al., 2013), especially in high NH_4^+ estuary and coastal sea, nitrate
136 assimilation may be inhibited in oxygenated water and, subsequently, so is the nitrite
137 release. Thus, the nitrite release was ignored in our model. Due to DIN assimilation by
138 phytoplankton, the PN pool may increase, but DON may be released during
139 assimilation (F5 in Fig. 1a and F7 in Fig. 1b) as indicated by previous studies (Bronk et

al., 1994; Bronk and Ward, 2000; Varela et al., 2005). On the other hand, remineralization may refuel the NH_4^+ pool (F2 in both Fig. 1a and 1b). Meanwhile, ammonium pool is reduced by nitrification process, which consists of two basic steps: the ammonia oxidation by archaea/bacteria (AOA/AOB) to nitrite (F4 in Fig. 1b) and the nitrite oxidation to nitrate by nitrite-oxidizing bacteria (NOB) (F6 in Fig. 1b). Although recent studies have revealed a single microorganism that may completely oxidize NH_4^+ to NO_3^- (comammox) (Daims et al., 2015; van Kessel et al., 2015), its importance in the marine environment remains unclear.

Specific mechanisms or processes such as grazing and viral lysis may alter the concentrations of NH_4^+, nitrite, and DON. However, the scope of this study is to determine the nitrogen flows and exchanges among the often measured and operationally defined nitrogen pools. In this context, grazers and viruses belong to the operationally defined PN and DON pools, respectively. Thus, the resultance of specific process such as grazing and viral lysis has been incorporated in the paradigm depicted in Figure 1.

2.2 Analytical methods to determine the amounts of $^{15}N/^{14}N$ in various pools

To trace the ^{15}N movement among pools, our isotope matrix method couples the ^{15}N-labelling and inventory methods through considering both concentration and isotopic composition changes. Analytical methods to determine the concentrations and isotopic compositions of both high and low levels of inorganic/organic nitrogen are in most cases well established and have been reported elsewhere. We determined all of the

161 mentioned concentrations and isotopic compositions except the isotopic composition of
162 NH_4^+.

163 Concentrations of NH_4^+ higher than 0.5 μM were measured manually by using the
164 colorimetric phenol hypochlorite technique (Koroleff, 1983). Nanomolar NH_4^+
165 concentrations were measured by using the fluorometric o-phthaldialdehyde (OPA)
166 method (Zhu et al., 2013). Concentrations of NO_2^- and NO_x^- (NO_2^- + NO_3^-) were
167 determined with the chemiluminescence method following the protocol of Braman and
168 Hendrix (1989). The detection limits of NO_2^- and NO_x^- were both ~ 10 nmol L^{-1}, and
169 the corresponding relative precision was better than 5% within the range of
170 concentrations that we measured. By using persulfate as an oxidizing reagent, we
171 oxidized TDN and PN separately to nitrate (Knapp et al., 2005) and then measured the
172 nitrate by using the analytical method for NO_x^- described above.

173 We determined the $\delta^{15}N$ of NO_2^- with the azide method by following the detailed
174 procedures in McIlvin and Altabet (2005). The $\delta^{15}N$ of NO_x^- was determined by using a
175 distinct strain of bacteria that lacked N_2O reductase activity to quantitatively convert
176 NO_x^- to nitrous oxide (N_2O), which we then analyzed by IRMS (denitrifier method;
177 (Sigman et al., 2001; Casciotti et al., 2002). The isotopic composition of NO_3^- was
178 determined from isotope mass balance (NO_x^- minus NO_2^-) or measured by the
179 denitrifier method after eliminating preexisting NO_2^- with sulfamic acid (Granger and
180 Sigman, 2009). To determine the $\delta^{15}N$ of TDN and PN, both species were first
181 converted to NO_3^- with the denitrifier method, and then the $\delta^{15}N$ of the NO_3^- was

182 determined as described above. The detection limit of $\delta^{15}N_{PN}$ can be reduced to
183 nanomole level (absolute amount of nitrogen), which is significantly lower than that
184 by using high temperature combustion with an elemental analyzer connected to
185 IRMS.

186 The most popular way to determine the N isotopic composition of NH_4^+ is the
187 "diffusion method", which involves conversion of dissolved NH_4^+ to NH_3 gas by
188 raising the sample pH to above 9 with magnesium oxide (MgO) and subsequently
189 trapping the gas quantitatively as $(NH_4)_2SO_4$ on a glass fiber (GF) filter; the isotope
190 ratios of the $^{15}N/^{14}N$ are then measured using a coupled elemental analyzer with an
191 IRMS (Holmes et al., 1998; Hannon and Böhlke, 2008). Alternatively, after removing
192 the preexisting NO_2^- from the seawater samples using sulfamic acid, NH_4^+ is first
193 quantitatively oxidized to NO_2^- by hypobromite (BrO^-) at pH ~12 (BrO^- oxidation
194 method), and the protocol of McIlvin and Altabet (2005) is then used to reduce the
195 NO_2^- to N_2O (Zhang et al., 2007). Unfortunately, neither of these methods has been
196 established in our lab yet. The isotope matrix method requires the isotopic composition
197 of NH_4^+ as well, but this requirement can be circumvented by making certain
198 assumptions, as illustrated in our case studies below.

199 We estimated the amount of ^{14}N and ^{15}N atoms in every individual pool for which
200 we knew the concentration and $\delta^{15}N$ ($\delta^{15}N$ ‰ = $[(R_{sample} - R_{atmN2})/R_{atmN2}] \times 1000$). By
201 assuming the ^{15}N content of standard atmospheric nitrogen to be 0.365%, we calculated
202 R_{sample} ($^{15}N/^{14}N$). By defining r_{sample} as $^{15}N/(^{14}N+^{15}N)$, we directly derived the ^{15}N and

203 ^{14}N concentrations of all forms of N, with the exception of NH_4^+ and DON. The r value
204 of the NH_4^+ was assumed to equal either its initial value or an arbitrarily chosen fraction
205 thereof, and the ^{15}N and ^{14}N content of the NH_4^+ was then determined.

206 **2.3 Formation of matrix equations**

207 In this isotope matrix method, we added limited amount of $^{15}NH_4^+$ into incubation
208 bottles at the very beginning and then monitored the changes of ^{15}N and ^{14}N in the
209 measured pools every a few hours. We assumed isotopic mass balance at every time
210 point in the incubation bottle. In other words, the sums of the variations in the total N,
211 ^{15}N, and ^{14}N concentrations were zero for any time interval. We assumed no
212 fractionation between ^{15}N and ^{14}N for all the transfer reactions among the pools. The
213 fluxes of ^{15}N and ^{14}N were therefore equal to the total flux multiplied, respectively, by
214 $r_{substrate}$ and $(1 - r_{substrate})$. Note that we did not consider isotope fractionation, though it
215 could easily be introduced into the equations if necessary, i.e., dividing ^{14}N flux by α
216 (the ratio of specific rate constant of ^{14}N to ^{15}N), and the flux of ^{15}N is obtained. Below,
217 we illustrated equations for the two model cases.

218 According to mass balance, the net changes of the ^{15}N (or ^{14}N) concentration of
219 individual N pool in certain time interval are determined by the inflow and outflow of
220 ^{15}N (or ^{14}N) (see Fig. 1 and Eqs. below). In the low-nitrogen case, the changes of the
221 ^{15}N concentrations of the NH_4^+, NO_x^-, and PN pools were expressed by Eq. 1, 2 and 3,
222 respectively. Similarly, the temporal dependence of ^{14}N-NH_4^+, ^{14}N-NO_x^-, and ^{14}N-PN
223 were expressed by Eq. 4, 5 and 6, respectively. The mean rate of change in nitrogen

pool, i.e. the left side of the equation, was determined from the data at time zero and the first time point. For example, when sampling time interval is short, $\Delta[^{14}NH_4^+]/\Delta t$ at the first time point was approximately $\{[^{14}NH_4^+]_{t1} - [^{14}NH_4^+]_{t0}\}/(t1-t0)$ where the subscripts indicate the times at which the concentrations were measured. The r value applied in the equation for substrate was the average of the r values at time zero and the first time point after that for measured pool.

$$\frac{\Delta\left[{}^{15}NH_4^+\right]}{\Delta T} = \overline{F_2} \times 0.00366 - \overline{F_1} \times \overline{r_{NH_4^+}} - \overline{F_3} \times \overline{r_{NH_4^+}} - \overline{F_6} \times \overline{r_{NH_4^+}} \quad (1)$$

$$\frac{\Delta\left[{}^{15}NO_x^-\right]}{\Delta T} = \overline{F_3} \times \overline{r_{NH_4^+}} - \overline{F_4} \times \overline{r_{NO_x^-}} \quad (2)$$

$$\frac{\Delta\left[{}^{15}PN\right]}{\Delta T} = \overline{F_1} \times \overline{r_{NH_4^+}} + \overline{F_4} \times \overline{r_{NO_x^-}} - \overline{F_5} \times \overline{r_{PN}} \quad (3)$$

$$\frac{\Delta\left[{}^{14}NH_4^+\right]}{\Delta T} = \overline{F_2} \times (1-0.00366) - \overline{F_1} \times (1-\overline{r_{NH_4^+}}) - \overline{F_3} \times (1-\overline{r_{NH_4^+}}) - \overline{F_6} \times (1-\overline{r_{NH_4^+}}) \quad (4)$$

$$\frac{\Delta\left[{}^{14}NO_x^-\right]}{\Delta T} = \overline{F_3} \times (1-\overline{r_{NH_4^+}}) - \overline{F_4} \times (1-\overline{r_{NO_x^-}}) \quad (5)$$

$$\frac{\Delta\left[{}^{14}PN\right]}{\Delta T} = \overline{F_1} \times (1-\overline{r_{NH_4^+}}) + \overline{F_4} \times (1-\overline{r_{NO_x^-}}) - \overline{F_5} \times (1-\overline{r_{PN}}) \quad (6)$$

In this study, we conducted a time series monitoring for over 24 hours, however, we took the first two time points for the rate calculation since such rate derivations might be more close to the instant rates in the original environments. Note: researchers may apply this method onto longer time interval, however, rates may vary as a result

of substrate consumption and/or community change, shorter-term incubation is suggested (see below).

Since the total number of equations and unknowns are equal, a unique solution therefore can be obtained via matrix solution for the low nutrient model.

In high nutrient cases, similarly, equations (Eqs. 7-14) can be constructed by using transformations among NH_4^+, NO_2^-, NO_3^- and PN (Fig. 1b).

$$\frac{\Delta\left[{}^{15}NH_4^+\right]}{\Delta T} = \overline{F_2} \times 0.00366 - \overline{F_1} \times \overline{r_{NH_4^+}} - \overline{F_4} \times \overline{r_{NH_4^+}} - \overline{F_8} \times \overline{r_{NH_4^+}} \quad (7)$$

$$\frac{\Delta\left[{}^{15}NO_2^-\right]}{\Delta T} = \overline{F_4} \times \overline{r_{NH_4^+}} - \overline{F_3} \times \overline{r_{NO_2^-}} - \overline{F_6} \times \overline{r_{NO_2^-}} \quad (8)$$

$$\frac{\Delta\left[{}^{15}NO_3^-\right]}{\Delta T} = \overline{F_6} \times \overline{r_{NO_2^-}} - \overline{F_5} \times \overline{r_{NO_3^-}} \quad (9)$$

$$\frac{\Delta\left[{}^{15}PN\right]}{\Delta T} = \overline{F_1} \times \overline{r_{NH_4^+}} + \overline{F_3} \times \overline{r_{NO_2^-}} + \overline{F_5} \times \overline{r_{NO_3^-}} - \overline{F_7} \times \overline{r_{PN}} \quad (10)$$

$$\frac{\Delta\left[{}^{14}NH_4^+\right]}{\Delta T} = \overline{F_2} \times (1 - 0.00366) - \overline{F_1} \times (1 - \overline{r_{NH_4^+}}) - \overline{F_4} \times (1 - \overline{r_{NH_4^+}}) - \overline{F_8} \times (1 - \overline{r_{NH_4^+}}) \quad (11)$$

$$\frac{\Delta\left[{}^{14}NO_2^-\right]}{\Delta T} = \overline{F_4} \times (1 - \overline{r_{NH_4^+}}) - \overline{F_3} \times (1 - \overline{r_{NO_2^-}}) - \overline{F_6} \times (1 - \overline{r_{NO_2^-}}) \quad (12)$$

$$\frac{\Delta\left[{}^{14}NO_3^-\right]}{\Delta T} = \overline{F_6} \times (1 - \overline{r_{NO_2^-}}) - \overline{F_5} \times (1 - \overline{r_{NO_3^-}}) \quad (13)$$

$$\frac{\Delta\left[{}^{14}PN\right]}{\Delta T} = \overline{F_1} \times (1 - \overline{r_{NH_4^+}}) + \overline{F_3} \times (1 - \overline{r_{NO_2^-}}) + \overline{F_5} \times (1 - \overline{r_{NO_3^-}}) - \overline{F_7} \times (1 - \overline{r_{PN}}) \quad (14)$$

Again, a unique solution can be obtained since the numbers of equations and unknowns are equal.

In the above matrix equations, r_{NH4+}, which we did not measure in this study, is necessary for the solution. Here we set various degrees of remineralization to test the effect of isotope dilution (NH_4^+ addition) in our experimental cases. We reduced r_{NH4+} values at a constant reduction rate and the total reduction of r_{NH4+} was 0%, 1%, 10%, 20% and 50% for the full time span of incubation (r_{NH4+} of remineralization is assumed to be 0.00366). The F2 coupled with given r_{NH4+} values allowed us to resolve rates under different remineralization conditions, and the derived F2 was introduced into STELLA model for extrapolations (see below). We compared the observed and remineralization-associated simulations to reveal the effect of remineralization on rate measure for time series incubations.

2.4 Validation by STELLA

As the aforementioned, the "instant rate" at the original condition is what researchers pursue. Note that the use of "instant" here is just to make it distinguishable from the longer time incubation or more than two time points. To evaluate the applicability of matrix-derived instant rate, here we applied STELLA 9.1.4 software (Isee systems, Inc.) to construct box models that were consistent with the scenarios depicted in Figure 1. The constructed STELLA model contained two modules (Figs. S1 and S2), one for ^{15}N and the other for ^{14}N. The connection between these two modules was through the ^{15}N atom % (rN), which was a measured parameter in the incubation

experiment. The model started to run with these measured initial values for nitrogen pools at time zero and to project continuous changes of corresponding nitrogen pools. Since the rate numbers based on the first two time points may not guarantee a good performance for the full time course due to system variation, i.e., changes in substrate concentration and microorganism community, we took this model practice (extrapolation) as a validation.

In this study, we assumed the first order reaction for both cases, thus, the initial rate constant "k" can be derived via dividing matrix-derived F by $\bar{C}$ (the average substrate concentration of the first two time points). After setting the initial concentrations of ^{15}N and ^{14}N to every pool, the model ran for 24 h according to matrix-derived short-term k values. As depicted in Figure 1, all these monitored N pools are regulated by F, which is concentration dependent according to our assumption (Figs. S1 and S2). The output includes the time courses of the ^{15}N and ^{14}N concentrations and the ^{15}N atom % (r_N) of each N species. Through this comparison, we could observe the course evolution of the isotopic composition in various N pools.

2.5 Study sites and incubation experiments

Incubation experiments were conducted in two environments with very different nutrient levels. The low nutrient case was conducted on-deck of the R/V Dongfanghong 2 on a cruise to the Western North Pacific (WNP) (33.3 °N, 145.9 °E) in spring 2015. The site for the high nutrient case is in the Wuyuanwan Bay (WYW) (24.5 °N, 118.2 °E) in the southern coast of China.

296 The water samples at WNP station were collected using a 24-bottle rosette
297 sampler. The sampling depth was 25 m with moderate light intensity (12% the surface
298 water irradiance). Two pre-washed 10-L polycarbonate carboys (Nalgene, USA) were
299 used for the incubation. A total of 1.5 mL of 200 μM ^{15}N-labelled NH_4Cl tracers
300 containing 98 atom% 15N (Sigma-Aldrich, USA) was injected into each incubation
301 bottle separately to achieve a final concentration of 30 nM. Incubation was carried out
302 immediately with a constant simulated light intensity (35 μmol E m^{-2} s^{-1}) in a
303 thermostatic incubator (GXZ-250A, Ningbo) at *in situ* temperature.

304 The WYW station is an inner bay with a regular semidiurnal tide. As a coastal bay,
305 Wuyuanwan suffers from anthropogenic influences that result in high nutrient
306 concentrations analogous to other coastal zones in China. However, the bay water is
307 still well ventilated and constantly saturated with dissolved oxygen due to tidally
308 induced water exchange. It is an ideal research site to study the dynamic transformation
309 processes of the coastal nitrogen cycle.

310 The WYW samples were taken on 19 January, 2014 from water depth of 0.3 m and
311 2.3 m, respectively, with a light intensity of 80 % and 2% of the surface water
312 irradiance. Duplicate water samples were collected for each depth by using submersible
313 pump into pre-washed 10-L polycarbonate bottles (Nalgene, USA). ^{15}N-labeled NH_4Cl
314 (98 atom % ^{15}N, Sigma-Aldrich, USA) was added to the incubation bottles with final
315 concentration of 1μM (~4 % of the ambient concentration). The incubations were
316 carried out immediately in the field. Neutral density-screen that allows 80% and 2%

light penetration was applied, respectively, for incubation bottles of shallow and deep samples. The temperature was maintained at ~13.7 ℃ by continuously pumped seawater throughflow.

Sample of the first time point (t0) was taken immediately after tracer addition. Subsequent samples were taken at approximately 2–4 h interval for DIN and PN analyses. An aliquot of 200 mL was filtered through a 47-mm polycarbonate membrane with a 0.22 μm pore size (Millipore, USA), and the filtrates were frozen at –20 ℃ for chemical analyses in the lab. Particulate matter was collected by filtering 500 ml seawater through pre-combusted (450 ℃ for 4 h) 25 mm GF/F filters (Whatman, GE Healthcare, USA), under a pressure of <100 mm Hg. The GF/F filters were freeze-dried and stored in a desiccator for PN concentration and isotopes.

3. Results

3.1 Ambient condition and initial concentrations

The water temperature and salinity of the WNP low nutrient case from 25m was 18.4 ℃ and 34.8, respectively. The dissolved oxygen (DO) was 7.3 mg L^{-1}. The concentration of NH_4^+, NO_x^- and phosphate was 113 ± 5 nmol L^{-1}, 521 ± 18 nmol L^{-1} and 74 ± 2 nmol L^{-1}, respectively. The N/P ratio was lower than 16, indicating the system is N limited.

The water temperature and salinity of the WYW whole water column for high nutrient case was 13.5 ± 0.1 ℃ and 29.5 ± 0.1, respectively. The DO saturation ranged 135-140%. The concentrations of nitrogenous species were relatively high with

inorganic nutrient concentrations of 30.9 ± 0.7 μmol L^{-1} for NO_3^-, 22.3 ± 4.3 μmol L^{-1} for NH_4^+, 5.4 ± 0.2 μmol L^{-1} for NO_2^-, and 9.3 ± 0.7 μmol L^{-1} for PN. Phosphate was 1.5 ± 0.1 μmol L^{-1}.

3.2 Time-courses of incubations

3.2.1 Low nutrient case

The observed variation patterns for the bulk NH_4^+, NO_x^-, PN, and TDN concentrations and $\delta^{15}N$ of NO_x^- and PN during incubation are shown in Figure 2. Concentrations of NH_4^+ and NO_x^- decreased rapidly from 143 ± 5 to 48 ± 5 nM and 521 ± 18 to 127 ± 11 nM, respectively (Figs. 2a and 2b). In contrast, PN concentration increased from 437 ± 9 to 667 ± 14 nM (Fig. 2c), and the TDN concentration remained stable, with an average of 6511 ± 209 nM (Fig. 2d). Opposite to the trend of NO_x^- concentration, $\delta^{15}N$-NO_x^- increased from 8.9 ± 0.2 to 171 ± 2 ‰ (Fig. 2e). In addition, $\delta^{15}N$-PN exhibited great changes, increasing from 46.8 ± 0.2 to 6950 ± 314 ‰ (Fig. 2f).

3.2.2 High nutrient cases

The time-series of observational parameters for samples from depths of 80% and 2% sPAR exhibited similar variation trends during incubation (Fig. 3). During the course of incubation, NH_4^+ decreased significantly and continuously from 26.6 ± 0.1 (initial concentration) to 17.4 ± 0.1 μmol L^{-1} with a mean reduction rate of 0.63 μmol L^{-1} h^{-1} for 80% sPAR sample (Fig. 3a). Compared with that of 80% sPAR, NH_4^+ of 2% sPAR sample decreased slower from 24.6 ± 0.1 (initial concentration) to 18.2 ± 1.0 μmol L^{-1}

with a mean reduction rate of 0.47 μmol L^{-1} h^{-1} (Fig. 3a). NO_3^- in 80% and 2% sPAR decreased from 30.1 ±0.1 to 28.3 ±0.1 μmol L^{-1} and from 31.1 ±0.1 to 29.7 ±0.1 μmol L^{-1}, respectively (Fig. 3c). Overall, the nitrate reduction rates were much lower than that of NH_4^+. Compared to nitrate, NO_2^- displayed even slower declining trends yet with significantly higher rate for 80% sPAR sample relative to that of 2% sPAR sample (Fig. 3b). Similar to the low nutrient case, PN increased steadily from 8.8 ±0.1 to 17.7 ±0.9 μmol L^{-1} with a mean rate of 0.61 μmol L^{-1} h^{-1} for 80% sPAR sample and from 9.9 ±0.1 to 16.0 ±2.0 μmol L^{-1} with a mean rate of 0.44 μmol L^{-1} h^{-1} in 2% sPAR (Fig. 3d). The increase rates in PN concentration were very close to the decrease rates of NH_4^+ indicating ammonium was the major nitrogen source for growth. The TDN concentration decreased from 78.7 ±1.6 to 68.4 ±0.1 μmol L^{-1} and form 72.8 ±2.5 to 67.1 ±0.8 μmol L^{-1} for 80% and 2% sPAR samples, respectively (Fig. 3e).

The δ^{15}N-NO_2^- increased from –9.0 ±0.1 to 12.1 ±0.1 ‰ and –8.8 ±0.1 to 23.3 ± 0.6 ‰ in 80% and 2% sPAR incubation, respectively (Fig. 3g); Since nitrate pool was relatively large, the values of δ^{15}N-NO_3^- ranged from 6.8 to 10.1 ‰ with no significant trend over time (Fig. 3h). In addition, δ^{15}N-PN increased from 14.8 ±0.3 to 3078 ±180 ‰ and from 15.0 ±0.5 to 2738 ±66 ‰ for 80% and 2% sPAR sample, respectively (Fig. 3i). These significant changes in both concentration and isotopic compositions of nitrogen pools over time suggested that nitrogen transformed significantly among pools and the labelled ^{15}N in NH_4^+ flowed through the system except nitrate.

3.3 Solutions of the matrix equation and STELLA extrapolation

3.3.1 Low nutrient case

The matrix-derived rate constants (ki) and rates (Fi) are shown in Table 1(A) and 1(B), respectively. Under no remineralization condition (i.e. r_{NH4+} decreased 0% within 24 hours), the NO_x^- uptake (k4= 0.059 h^{-1}; F4 = 27.2 nmol L^{-1} h^{-1}) was the highest among all in terms of flux, followed by NH_4^+ uptake (k1 = 0.038 h^{-1}; F1 = 4.9 nmol L^{-1} h^{-1}) and DON release (k5= 0.024 h^{-1}; F5 = 11.5 nmol L^{-1} h^{-1}). NH_4^+ uptake by bacteria (k6 = 0.007 h^{-1}; F6 = 1.0 nmol L^{-1} h^{-1}) was much lower than that by phytoplankton. The rate constant for nitrification (k3 = 0.0005 h^{-1}) was the lowest among all fluxes (F3 = 0.07 nmol L^{-1} h^{-1}).

By introducing initial ^{15}N and ^{14}N concentrations of NH_4^+, NO_x^-, PN and DON and the calculated rate constants (k1 to k6) into STELLA (Fig. S1), we obtained full time courses for all parameters (Fig. 4). Generally, the model outputs fitted well with the measured values except the last time point for PN associated ^{15}N concentration, $\delta^{15}N$, and r_N (Figs. 4 c, k and o). In general, the rates of the first time interval can well predict the following up observations, demonstrating a good predictive performance by using the matrix method instant rate. Since both substrates, e.g., ammonium and NO_x^-, fitted well within 24 hours, the extra non-fitted PN in observation after the time point of 12 hours likely indicated the participation of an additional nitrogen source, i.e., dissolved organic nitrogen that was utilized by phytoplankton (see discussion below) when inorganic nitrogen reached threshold levels (Sunda and Ransom, 2007).

In these test runs of regeneration with r_{NH4+} reduction by a total amount of 1 %, 10 %, 20 % and 50 %, we found that the NH_4^+ consumption rates (k1 and k6) increased as the regeneration (k2) increased (Table 1). As indicated in previous studies, such regeneration-induced isotope dilution indeed altered the original results (Table 1 and Fig. 4). More specifically, greater NH_4^+ regeneration resulted in larger differences between these three PN-associated values (^{15}N-PN, δ^{15}N-PN, and r_{PN}) and the STELLA-projected data (Figs. 4 c, k and o). Meanwhile, the dilution effect was more significant after 12 hours of incubation. On the other hand, the effect of r_{NH4+} on NO_x^- -associated parameters was trivial (Figs. 4 b, f, j, n and r). The comparison between the simulation and observation suggested that NH_4^+ regeneration needs to be considered for PN (i.e., uptake) when remineralization rate is high and incubation prolongs. Besides remineralization, offsets along the time course might possibly be induced by the community change as incubation prolongs.

3.3.2 High nutrient cases

The results of 80% sPAR and 2% sPAR under the assumption of fixed r_{NH4+} are shown in Table 2(A) and 2(B), respectively. For the high light sample (80 % sPAR), the NH_4^+ uptake by phytoplankton (F1, 397 nmol L^{-1} h^{-1}) and by bacteria (F8, 282 nmol L^{-1} h^{-1}) were much higher than the other rates and were followed by the NO_3^- uptake rate (F5, 149 nmol L^{-1} h^{-1}). The NO_2^- uptake (F3) rate was 29 nmol L^{-1} h^{-1}, much lower than that of NH_4^+ and NO_3^- uptake. The ammonia oxidation rate (F4) was 0.4 nmol L^{-1} h^{-1}, and the nitrite oxidation rate (F6) was zero (Table 2A). Since this incubation was

conducted in winter with low temperature and under 80% sPAR light conditions, low rates of ammonium and nitrite oxidation were reasonable because both nitrifiers and NOB are sensitive to light (e.g. Olson, 1981a, 1981b; Horrigan et al., 1981; Ward, 2005; Merbt et al., 2012; Smith et al., 2014). The DON release rate by phytoplankton (F7) was zero in this case.

In comparison, all the rates in the condition of 2% sPAR showed a very similar pattern (Table 2B). The only difference was that all the uptake rates were lower for the 2% sPAR except for ammonia oxidation, which was higher in the low light.

By introducing initial concentrations and calculated rate constants (k1–k8) into the STELLA model (Fig. S2), we obtained successive variations of ^{15}N and ^{14}N concentrations and r_N of NH_4^+, NO_2^-, NO_3^-, PN and DON over time (Fig. 5). In general, the modeled and measured values remained consistent throughout the 15 h incubation, demonstrating the capability of the isotope matrix method.

Similar to the low nutrient case, we evaluated the effect of regeneration (see Table 2 and Fig. 5A and 5B). Since ammonium uptake was the dominant process, the alteration of the PN pool was more significant in comparison with the other pools (Figs. 5 d, n and s). We found again, as F2 increased, F1 and F8 increased to maintain a constant reduction of the measured NH_4^+ concentration (Table 2). Similar to low nutrient case, as regeneration increased the projected course of ^{15}N-PN deviated more from observation and the turning point also appeared earlier, resulting in a larger curvature of r-PN and $\delta^{15}N$-PN (Fig. 5d and 5s). This model exercise confirmed the

441 influence of the isotope dilution effect; however, the effect is insignificant in the early
442 stage of incubation.

443 # 4. Discussion

444 ## 4.1 Method comparisons

445 ### 4.1.1 Model structure and rate derivation

446 The most widespread ^{15}N model was proposed by Dugdale and Goering (1967),
447 who assumed the isotopic and mass balances in the particulate fraction, resulting in the
448 commonly used formula for nitrogenous nutrient uptake. Dugdale and Wilkerson
449 (1986) modified their rate equations further and highlighted the importance of
450 short-term incubation. Although short-term incubation was requested, Collos (1987)
451 demonstrated that the formula based on the concentration of particles at the end of the
452 experiment, rather than at the beginning, is more reliable when more than one N source
453 are simultaneously incorporated by the phytoplankton population. That is, the equation
454 by Collos (1987) corrected the bias caused by unlabeled multiple N utilization.

455 Different from the above mentioned equations, Blackburn (1979) and Caperon et
456 al. (1979) proposed ^{15}N isotope dilution models based on the substrate rather than
457 product. By measuring the isotope values and concentrations of the substrate, e.g. NH_4^+,
458 and then both NH_4^+ consumptions (DON and/or PN as product) and regeneration rate
459 can be obtained. Glibert et al. (1982) further modified the isotope dilution method and
460 calculated the uptake rate into PN fraction by substituting the exponential average r_{NH4+}

461 at the beginning and at the end of incubation to correct the isotope dilution existing in
462 the model of Dugdale and Goering (1967). Besides method improvements, imbalance
463 was often observed between the substrate reduction and the increase in particulate
464 phase in field studies. Laws (1985) introduced a new model with consideration of the
465 imbalance and calculated the "net uptake rate" (into PN). Later on, Bronk and Glibert
466 (1991) revised Law's model on the basis of the model proposed by Glibert et al. (1982)
467 to calculate the "gross uptake rate" (substrate incorporation into PON plus DON).
468 Overall speaking, none of the above models considered mass balance at whole system
469 scale. Although rates were obtained via analytical solutions, the bias potential due to
470 multiple flows was not completely solved.

471 To solve multiple co-occurring N processes, Elskens et al. (2002) formulated a
472 new model, containing 3n+1 equations (n stands for the number of labelled N
473 substrate) and 3n+1 flux rates, by taking multiple co-occurring N fluxes in natural
474 system into account. Approximate rates in their model were resolved by a weighted
475 least squares technique. Additionally, Elskens et al. (2005) created a process-oriented
476 model (PROM) accounting for as many N processes as needed to quantify how
477 specific underlying assumptions affect the estimation behavior of all above-mentioned
478 models. The authors concluded uncertainties may increase as the incubation prolongs
479 and oversimplified models may risk bias when their underlying assumptions are
480 violated. The most recent attempt to resolve simultaneous N processes was conducted
481 by Pfister et al. (2016) who applied parallel incubations (^{15}N labelled NH_4^+ and NO_3^-)

in tidepools to measure multiple flows among benthic, ammonium, nitrite and nitrate pools. In their experiment, six differential equations (with seven unknowns) were constructed basing on mass and isotope balances and solved by using the ODE function of R language. Since benthic algae were not measured due to difficulty in sampling and spatial heterogeneity in biomass, the whole system scale mass balance cannot be reached; thus, the flux of DON release cannot be obtained.

Compared with methods or models mentioned above, the advantages of isotope matrix method include (1) the potential biases caused by multi-flows were considered under the circumstance of mass balance at system scale; (2) one tracer addition for multiple *in situ* flows (parallel incubations, i.e., dark and light or $^{15}NH_4^+$ and $^{15}NO_x^-$, were not needed); (3) simple post-hoc data processing and unique solution can be obtained via matrix derivation; (4) no extra laboratory work is demanded (see below).

4.1.2 Rate comparisons

Following Pfister et al. (2016), we estimated all N transformation rates via ODE for the three cases on the assumption that there is no remineralization for comparison (see Table 1−3). In general, the rate values obtained by the matrix and ODE were consistent. The rate difference, if any, was caused by the duration for integration, i.e., shorter time (the first two time points for calculation) for isotope matrix method and longer time (4 or 5 points for the entire incubation) for ODE. In Pfister et al. (2016), 3 monitoring points within 5 hours were implemented for ODE. Unfortunately, such intensive sampling for on-deck incubation is not practical; however, we still strongly

503 recommend the short-term incubation for water column study as previously suggested.
504 With proper duration, two time points for integration may be more convenient and
505 realistic for instant rate measure.

506 Below, we present a comparison with conventional source-product rate
507 measurements (Collos, 1987) of ammonium oxidation and uptake (Table 3). The
508 matrix-derived NH_4^+ uptake rates for all experimental cases were consistent with those
509 (difference < 8%) from the traditional source-product method when the final PN
510 concentration was applied for calculation. The deviations were larger (13−21%) when
511 the initial PN was applied, which was supported by the conclusion of previous studies
512 that estimate involving the final PN concentration more reliable. Obviously, deviation
513 could be higher when the phytoplankton growth rate was higher.

514 On the other hand, the end-products of ammonium oxidation or nitrification are
515 consumed by phytoplankton continuously, particularly in euphotic layer full of
516 photosynthetic autotrophs. In many cases, nitrate uptake occurs in both light and dark
517 conditions (e.g. Dugdale and Goering, 1967; Lipschultz, 2002; Mulholland and Lomas,
518 2008). The significant consumption of end-products (NO_x^- and NO_2^-) apparently
519 violate the underlying assumption of source-product rate calculation. Therefore, the
520 NH_4^+ oxidation/nitrification rate could not be obtained, such as all cases in our study
521 since phytoplankton consumption resulted in a net reduction of NO_x^- (Figs. 2b, 3b and
522 3c) (see Table 3).

In most cases, the final isotopic composition rather than final concentration of NO_x^- was measured; as such, researchers may not be aware of the greater $^{15}NO_x^-$ outflow than inflow. For dark incubation, researchers may also assume insignificant NO_x^- consumption. However, the "net decrease in end-product" is almost unavoidable when incubation is conducted under simulated *in situ* light condition for ammonium oxidation. To overcome this consumption effect induced by the first-order reaction, Santoro et al. (2010, 2013) took NO_x^- removal into account and formulated a new equation, a function of nitrification rate (F) and NO_x^- uptake rate (k). Following Santoro et al. (2010), we calculated the nitrification rate for the low-nutrient case (via a nonlinear least-squares curve-fitting routine in Matlab by using the first three time points of the $^{15}N\text{-}NO_x^-$ /$^{14}N\text{-}$ NO_x^-measurements) to be 0.05 nmol L^{-1} h^{-1} (Table 3), which was (~30%) lower than the matrix-derived rate (0.07 nmol L^{-1} h^{-1}). By contrast, their nitrate uptake rate (k = 0.010 h^{-1}) was only one-sixth of that (0.059 h^{-1}) derived from the matrix method, although a comparable nitrification rate was obtained when the consumption term was taken into account.

Surprisingly, when we introduced the two parameters by using the method of Santoro et al. (2010) into STELLA to generate the time courses of parameters, we found simulations of $\delta^{15}NO_x^-$ and r_{NOx-} agreed well with that of isotope matrix method (Figs. 4j and 4n), yet, much slower decreasing trends were found for $^{15}NO_x^-$, $^{14}NO_x^-$, and NO_x^- (Figs. 4 b, f and r). Finally, we realized that the formula produced by Santoro et al. (2010) is constrained only by the ratio changes rather than the individual

concentration changes in $^{15}NO_x^-$ and $^{14}NO_x^-$. Thus, the nonlinear curve-fitting method by Matlab may only provide a correct simulation for the ratio change. This implies that the nitrate uptake rate derived from the non-linear curve-fitting method in Matlab should be validated also by the final concentration of nitrate, as was done by Santoro et al. (2013).

In summary, (1) an accurate measurement of concentration time series is vital for all kinds of transformation rate estimate including the isotope matrix method and (2) the isotope matrix method overcame various biases that traditional methods might encounter.

4.2 Implications for nitrogen biogeochemical processes

Through the isotope matrix method, biogeochemical implications were obtained from various aspects.

4.2.1 Remineralization, regeneration and community succession

The matrix solution fit well with the model runs with variable r-NH_4^+ in early stage, suggesting that dilution effect was negligible during the early incubation period at least in our case. Dilution effect could be significant when remineralization is intensive and incubation prolongs. Pfister et al. (2016) found macrofauna (mussel) play an important role in remineralization. While zooplankton in the water column of our sampled cases was not abundant, it might be a reason for low remineralization rates in our short-term incubation.

In the WNP low nutrient case, after 24-hour incubation the levels of nitrate and ammonium approached the concentration threshold for phytoplankton utilization (e.g., <30−40 nM NH_4^+ for *Emiliania huxleyi*; Sunda and Ransom, 2007). In Figure 4, STELLA projection fitted well with PN parameters only for the first 12 hours. In this case, in fact, we have observed phytoplankton succession. Our flow cytometry data (shown in authors reply for Reviewer #2) demonstrated that the cell number of living eukaryotes (4 times higher than *Synechococcus*) increased in the first 24 hours and started to drop rapidly after 24 hours. On the contrary, the growth of *Synechococcus* continued throughout 94 hours under constantly low nitrogen nutrient situation. Such phenomenon suggested that phytoplankton community competed for nitrogen source and a major community shift started at around 24 hours. After the time point of 12 hours, observed parameters associated with PN was higher than the projection by STELLA. The most intriguing phenomenon among PN associated parameters was the additional ^{15}N, which should not come from $^{15}NH_4^+$, in PN. The most likely nitrogen source candidate with enriched ^{15}N to support *Synechococcus* growth was the nitrogen released from dead eukaryotes, which contained freshly consumed ^{15}N tracer, rather than the ambient DON. More studies are needed to explore nutrient thresholds for different phytoplankton species. Nevertheless, our results suggested that short-term incubation is crucial for nitrogen uptake studies in oligotrophic ocean.

4.2.2 Evaluate the contribution of nitrification to new production

584 Nitrification in the sunlit ocean drew not much attention until recent decades after
585 the widespread ammonia oxidizing archaea (AOA) discovery in the perspective of
586 molecular evidence (Francis et al., 2005; Santoro et al., 2010, 2013; Smith et al., 2014)
587 and rate measurements based on isotope (Ward, 2011; Santoro et al., 2010; Grundle et
588 al., 2013; Smith et al., 2014). As mentioned in Introduction, the conventional "new"
589 production has been overestimated 19−33% on a global scale due to the "regenerated"
590 nitrate via nitrification process. However, a more realistic evaluation for the fractional
591 contribution of nitrification to NO_3^- uptake can only be achieved when the incubation
592 is conducted in the same bottle under *in situ* light conditions instead of parallel
593 incubations in dark and light. The isotope matrix method is so far the most convenient
594 and suitable method for evaluating the relative importance of co-occuring nitrification
595 and new production in the euphotic ocean. In all our experimental cases, the
596 contributions of nitrification to new production were < 1% (Table 4). The relatively
597 low contribution was probably due to the light inhibition on nitrifiers for the WNP case
598 and because of the low temperature in the sampling season.
599 Nevertheless, light effect in our case studies is significant. Light suppresses
600 nitrification (Ward, 2005; Merbt et al., 2012; Peng et al., 2016). NH_4^+ oxidation rate in
601 80% sPAR reduced by 36% relative to that in 2% sPAR. Results agreed with current
602 knowledge although some recent evidences showed that some taxa of marine AOA
603 hold genetic capabilities to reduce oxidative stress and to repair ultraviolet damage
604 (Luo et al., 2014; Santoro et al., 2015). More study cases are needed in the future to

605 explore vertical distributions of the relative contribution of nitrification to new
606 production in euphotic zone.

607 **4.2.3 Nutrient preference**

608 Phytoplankton takes different nitrogenous species as nutrients for growth.
609 McCarthy et al. (1977) introduced a relative preference index (PRI) to assess the
610 relative utilization of a specific N form, and when RPI value >1 indicates a preference
611 for the specific substrate over the other N forms. As shown in Table 4, in the NO_3^-
612 prevailed low nutrient case, the PRI (NO_3^-) was very close but slightly higher to PRI
613 (NH_4^+), which was probably due to the phytoplankton community structure as
614 mentioned above. This result was in line with the result in the Sargasso Sea (Fawcett et
615 al., 2011). While in the high NH_4^+ bay, the PRI (NH_4^+) > 1 > PRI (NO_3^-) > PRI (NO_2^-),
616 suggesting that phytoplankton preferred NH_4^+ over NO_3^- and NO_2^-, similar to the result
617 in Chesapeake Bay (McCarthy et al., 1977).

618 **4.2.4 Quantify various ammonium consumption pathways**

619 In the upper ocean, NH_4^+ cycles rapidly due to various microorganisms's
620 metabolic pathways competing for ammonium. Ammonium may serve as nitrogen
621 source for phytoplankton assimilation, and as energy source for ammonia oxidizing
622 organisms (AOM). Moreover, many studies have shown that bacteria also play a part in
623 NH_4^+ utilization (Middelburg and Nieuwenhuize, 2000; Veuger et al., 2004). Our result
624 in the low nutrient case showed that phytoplankton was the main NH_4^+ consumer (82%

625 of the total NH_4^+ consumption), bacteria accounted for another ~17% and AOM
626 utilized the rest 1%. While in the eutrophic WYW bay, phytoplankton and bacteria
627 each consumed ~50% of the total NH_4^+ (Table 4).

628 5. Conclusion

629 This isotope matrix method was designed specifically for euphotic water column
630 incubation under simulated *in situ* condition. By considering multi-flows among pools
631 on the assumption of mass balance at the whole system level, we minimized potential
632 biases caused by non-targeted processes in traditional source-product methods. Given
633 the progress in analytical techniques for concentration and isotopic composition of
634 nitrogen species, the isotope matrix method presents a promising avenue for the study
635 of rates of nitrogen processes with a system-wide perspective. Furthermore, the
636 matrix method is also appropriate for probing the effects of environmental factors (e.g.,
637 CO_2, pH, temperature, and light intensity) on the interactive N processes in one single
638 incubation bottle.

639 Acknowledgement

640 We sincerely thank Wenbin Zou and Tao Huang at the State Key Laboratory of
641 Marine Environmental Science (Xiamen University, China) for their valuable help with
642 the water sampling and the on-board trace NH_4^+ concentration analysis during the 2015
643 NWP cruise. Yu-ting Shih from the Department of Geology at National Taiwan
644 University in Taiwan is thanked for his help on ODE application. This research was

funded by the National Natural Science Foundation of China (NSFC U1305233, 2014CB953702, 91328207, 2015CB954003).

References

Beman, J. M., Popp, B. N., and Alford, S. E.: Quantification of ammonia oxidation rates and ammonia-oxidizing archaea and bacteria at high resolution in the Gulf of California and eastern tropical North Pacific Ocean, Limnol. Oceanogr., 57, 711-726, doi:10.4319/lo.2012.57.3.0711, 2012.

Blackburn, T. H.: Method for Measuring Rates of NH_4^+ Turnover in Anoxic Marine Sediments, Using a ^{15}N-NH_4^+ Dilution Technique, Appl. Environ. Microbiol., 37, 760-765, 1979.

Braman, R. S., and Hendrix, S. A.: Nanogram nitrite and nitrate determination in environmental and biological materials by vanadium (III) reduction with chemiluminescence detection, Anal. Chem., 61, 2715-2718, doi: 10.1021/ac00199a007, 1989.

Brauwere, A. D., Ridder, F. D., Pintelon, R., Elskens, M., Schoukens, J., and Baeyens, W.: Model selection through a statistical analysis of the minimum of a weighted least squares cost function, Chemom. Intell. Lab. Syst., 76, 163-173, doi:10.1016/j.chemolab.2004.10.006, 2005.

Bronk, D., Killberg-Thoreson, L., Sipler, R., Mulholland, M., Roberts, Q., Bernhardt, P., Garrett, M., O'Neil, J., and Heil, C.: Nitrogen uptake and regeneration (ammonium regeneration, nitrification and photoproduction) in waters of the West Florida Shelf prone to blooms of Karenia brevis, Harmful Algae, 38, 50-62, doi:10.1016/j.hal.2014.04.007, 2014.

Bronk, D. A., and Glibert, P. M.: A ^{15}N tracer method for the measurement of dissolved organic nitrogen release by phytoplankton. Mar. Ecol. Prog. Ser., Marine Ecology Progress, 77, 1991.

Bronk, D. A., Glibert, P. M., and Ward, B. B.: Nitrogen uptake, dissolved organic nitrogen release, and new production, Science, 265, 1843-1846, 1994.

Bronk, D. A., and Ward, B. B.: Magnitude of dissolved organic nitrogen release relative to gross nitrogen uptake in marine systems, Limnol. Oceanogr., 45, 1879-1883, doi: 10.4319/lo.2000.45.8.1879, 2000.

676 Caperon, J., Schell, D., Hirota, J., and Laws, E.: Ammonium excretion rates in Kaneohe
677 Bay, Hawaii, measured by a ^{15}N isotope dilution technique, Mar. Biol., 54, 33-40, doi:
678 10.1007/BF00387049, 1979.

679 Casciotti, K., Sigman, D., Hastings, M. G., Böhlke, J., and Hilkert, A.: Measurement of
680 the oxygen isotopic composition of nitrate in seawater and freshwater using the
681 denitrifier method, Anal. Chem., 74, 4905-4912, 2002.

682 Casciotti, K. L.: Nitrogen and Oxygen Isotopic Studies of the Marine Nitrogen Cycle,
683 Ann. Rev. Mar. Sci., 8, 379-407, doi: 10.1146/annurev-marine-010213-135052, 2016.

684 Chen, Y.-l. L.: Spatial and seasonal variations of nitrate-based new production and
685 primary production in the South China Sea, Deep Sea Res. Part I Oceanogr. Res. Pap.,
686 52, 319-340, doi:10.1016/j.dsr.2004.11.001, 2005.

687 Collos, Y.: Calculations of ^{15}N uptake rates by phytoplankton assimilating one or
688 several nitrogen sources, International Journal of Radiation Applications and
689 Instrumentation. Part A. Applied Radiation and Isotopes, 38, 275-282,
690 doi:10.1016/0883-2889(87)90038-4, 1987.

691 Daims, H., Lebedeva, E. V., Pjevac, P., Han, P., Herbold, C., Albertsen, M., Jehmlich,
692 N., Palatinszky, M., Vierheilig, J., Bulaev, A., Kirkegaard, R. H., von Bergen, M.,
693 Rattei, T., Bendinger, B., Nielsen, P. H., and Wagner, M.: Complete nitrification by
694 Nitrospira bacteria, Nature, 528, 504-509, 10.1038/nature16461,
695 doi:10.1038/nature16461, 2015.

696 Dugdale, R., and Goering, J.: Uptake of new and regenerated forms of nitrogen in
697 primary productivity, Limnol. Oceanogr., 12, 196-206, doi: 10.4319/lo.1967.12.2.0196,
698 1967.

699 Dugdale, R., and Wilkerson, F.: The use of ^{15}N to measure nitrogen uptake in eutrophic
700 oceans; experimental considerations, Limnol. Oceanogr., 31, 673-689, doi:
701 10.4319/lo.1986.31.4.0673, 1986.

702 Elskens, M., Baeyens, W., Cattaldo, T., Dehairs, F., and Griffiths, B.: N uptake
703 conditions during summer in the Subantarctic and Polar Frontal Zones of the Australian
704 sector of the Southern Ocean, J. Geophys. Res.: Oceans, 107, 3-1-3-11,
705 doi:10.1029/2001JC000897, 2002.

706 Elskens, M., Baeyens, W., Brion, N., Galan, S. D., Goeyens, L., and Brauwere, A. D.:
707 Reliability of N flux rates estimated from ^{15}N enrichment and dilution experiments in
708 aquatic systems, Global Biogeochem. Cycles, 19, 573-574,
709 doi:10.1029/2004GB002332, 2005.

710 Falkowski, P. G.: Evolution of the nitrogen cycle and its influence on the biological
711 sequestration of CO_2 in the ocean, Nature, 387, 272-275, doi: 10.1038/387272a0, 1997.

712 Fawcett, S. E., Lomas, M. W., Casey, J. R., Ward, B. B., and Sigman, D. M.:
713 Assimilation of upwelled nitrate by small eukaryotes in the Sargasso Sea, Nature
714 Geoscience, 4, 717-722, doi:10.1038/ngeo1265, 2011.

715 Francis, C. A., Roberts, K. J., Beman, J. M., Santoro, A. E., and Oakley, B. B.: Ubiquity
716 and diversity of ammonia-oxidizing archaea in water columns and sediments of the
717 ocean, Proceedings of the National Academy of Sciences, 102, 14683-14688, doi:
718 10.1073/pnas.0506625102, 2005.

719 Gilbert, P. M., Lipschultz, F., McCarthy, J. J., and Altabet, M. A.: Isotope dilution
720 models of uptake and remineralization of ammonium by marine plankton, Limnol.
721 Oceanogr., 27, 639-650, 1982.

722 Granger, J., and Sigman, D. M.: Removal of nitrite with sulfamic acid for nitrate N and
723 O isotope analysis with the denitrifier method, Rapid Commun. Mass Spectrom., 23,
724 3753-3762, 10.1002/rcm.4307, doi: 10.1002/rcm.4307, 2009.

725 Grundle, D. S., Juniper, S. K., and Giesbrecht, K. E.: Euphotic zone nitrification in the
726 NE subarctic Pacific: Implications for measurements of new production, Mar. Chem.,
727 155, 113-123, doi:10.1016/j.marchem.2013.06.004, 2013.

728 Hannon, J. E., and Böhlke, J. K.: Determination of the delta ($^{15}N/^{14}N$) of Ammonium
729 (NH_4^+) in Water: RSIL Lab Code 2898, US Geological Survey 2328-7055, 2008.

730 Harrison, P. J., and Davis, C. O.: Use of the perturbation technique to measure nutrient
731 uptake rates of natural phytoplankton populations, Deep Sea Res., 24, 247-255,
732 doi:10.1016/S0146-6291(77)80003-9, 1977.

733 Harvey, W. A., and Caperon, J.: The rate of utilization of urea, ammonium, and nitrate
734 by natural populations of marine phytoplankton in a eutrophic environment, Pacific
735 Science, 30 (4), 329-340, http://hdl.handle.net/10125/1169, 1976.

736 Holmes, R., McClelland, J., Sigman, D., Fry, B., and Peterson, B.: Measuring $^{15}N–NH_4^+$
737 in marine, estuarine and fresh waters: An adaptation of the ammonia diffusion
738 method for samples with low ammonium concentrations, Mar. Chem., 60, 235-243,
739 doi:10.1016/S0304-4203(97)00099-6, 1998.

740 Horrigan, S., Carlucci, A., and Williams, P.: Light inhibition of nitrification in
741 sea-surface films [California], J. Mar. Res., 1981.

742 Howard, M. D. A., Cochlan, W. P., Ladizinsky, N., and Kudela, R. M.: Nitrogenous
743 preference of toxigenic Pseudo-nitzschia australis (Bacillariophyceae) from field and
744 laboratory experiments, Harmful Algae, 6, 206-217, doi:10.1016/j.hal.2006.06.003,
745 2007.

746 Hsiao, S.-Y., Hsu, T.-C., Liu, J.-w., Xie, X., Zhang, Y., Lin, J., Wang, H., Yang, J.-Y.,
747 Hsu, S.-C., and Dai, M.: Nitrification and its oxygen consumption along the turbid

748 Chang Jiang River plume, Biogeosciences, 11, 2083-2098,
749 doi:10.5194/bg-11-2083-2014, 2014.

750 Knapp, A. N., Sigman, D. M., and Lipschultz, F.: N isotopic composition of dissolved
751 organic nitrogen and nitrate at the Bermuda Atlantic Time-series Study site, Global
752 Biogeochem. Cycles, 19, doi: 10.1029/2004GB002320, 2005.

753 Koroleff, F.: Simultaneous oxidation of nitrogen and phosphorus compounds by
754 persulfate, Methods of seawater analysis, 2, 205-206, 1983.

755 Laws, E. A.: Analytic Models of NH_4^+ Uptake and Regeneration Experiments, Limnol.
756 Oceanogr., 30, 1340–1350, 1985.

757 Lipschultz, F.: A time-series assessment of the nitrogen cycle at BATS, Deep Sea Res.
758 Part II Top. Stud. Oceanogr., 48, 1897-1924, doi:10.1016/S0967-0645(00)00168-5,
759 2001.

760 Lipschultz, F.: Isotope Tracer Methods for Studies of the Marine Nitrogen Cycle, in
761 Nitrogen in the marine environment, edited by: Capone, D. A., Bronk, D. A.,
762 Mulholland, M. R., Carpenter, E. J., Academic Press, London, U.K., 303-384, 2008.

763 Lomas, M. W., and Lipschultz, F.: Forming the primary nitrite maximum: Nitrifiers or
764 phytoplankton?, Limnol. Oceanogr., 51, 2453-2467, doi: 10.4319/lo.2006.51.5.2453,
765 2006.

766 Luo, H., Tolar, B. B., Swan, B. K., Zhang, C. L., Stepanauskas, R., Ann, M. M., and
767 Hollibaugh, J. T.: Single-cell genomics shedding light on marine Thaumarchaeota
768 diversification, ISME Journal, 8, 732-736, doi:10.1038/ismej.2013.202, 2014.

769 Marchant, H. K., Mohr, W., Kuypers, M. M. M.: Recent advances in marine N-cycle
770 studies using ^{15}N labeling methods. Curr. Opin. Biotechnol., 41, 53-59,
771 doi:10.1016/j.copbio.2016.04.019, 2016.

772 McCarthy, J. J., and Eppley, R. W.: A comparison of chemical, isotopic, and enzymatic
773 methods for measuring nitrogen assimilation of marine phytoplankton, Limnol.
774 Oceanogr., 17, 371-382, doi: 10.4319/lo.1972.17.3.0371, 1972.

775 Mccarthy, J. J., Taylor, and Taft, J. L.: Nitrogenous nutrition of the plankton in the
776 Chesapeake Bay.1. Nutrient availability and phytoplankton preferences, Limnol.
777 Oceanogr., 22, 996-1011, 1977.

778 McIlvin, M. R., and Altabet, M. A.: Chemical conversion of nitrate and nitrite to nitrous
779 oxide for nitrogen and oxygen isotopic analysis in freshwater and seawater, Anal.
780 Chem., 77, 5589-5595, doi: 10.1021/ac050528s, 2005.

781 Merbt, S. N., Stahl, D. A., Casamayor, E. O., Mart ́ı E., Nicol, G. W., and Prosser, J. I.:
782 Differential photoinhibition of bacterial and archaeal ammonia oxidation, FEMS

783 Microbiol. Lett., 327, 41-46, doi: http://dx.doi.org/10.1111/j.1574-6968.2011.02457.x,
784 2012.

785 Middelburg, J. J., and Nieuwenhuize, J.: Uptake of dissolved inorganic nitrogen in
786 turbid, tidal estuaries, Mar. Ecol. Prog. Ser., 192, 79-88, doi:10.3354/meps192079,
787 2000.

788 Mulholland, M. R., and Lomas, M. W.: Nitrogen uptake and assimilation, in Nitrogen
789 in the marine environment, edited by: Capone, D. A., Bronk, D. A., Mulholland, M. R.,
790 Carpenter, E. J., Academic Press, London, U.K., 303-384, 2008.

791 Newell, S. E., Fawcett, S. E., and Ward, B. B.: Depth distribution of ammonia oxidation
792 rates and ammonia-oxidizer community composition in the Sargasso Sea, Limnol.
793 Oceanogr., 58, 1491-1500, doi:10.4319/lo.2013.58.4.1491, 2013.

794 Olson, R.: ^{15}N tracer studies of the primary nitrite maximum, J. Mar. Res., 39, 203-226,
795 1981a.

796 Olson, R. J.: Differential photoinhibition of marine nitrifying bacteria: a possible
797 mechanism for the formation of the primary nitrite maximum, J. Mar. Res., 39, 227-238,
798 1981b.

799 Painter, S. C., Patey, M. D., Tarran, G. A., and Torres-Valdés, S.: Picoeukaryote
800 distribution in relation to nitrate uptake in the oceanic nitracline, Aquat. Microb. Ecol.,
801 72, 195-213, doi:10.3354/ame01695, 2014.

802 Pakulski, J., Benner, R., Amon, R., Eadie, B., and Whitledge, T.: Community
803 metabolism and nutrient cycling in the Mississippi River plume: evidence for intense
804 nitrification at intermediate salinities, Mar. Ecol. Prog. Ser., 117, 207, 1995.

805 Peng, X., Fuchsman, C. A., Jayakumar, A., Warner, M. J., Devol, A. H., and Ward, B.
806 B.: Revisiting nitrification in the eastern tropical South Pacific: A focus on controls, J.
807 Geophys. Res.: Oceans, doi: 10.1002/2015JC011455, 2016.

808 Pfister, C. A., Altabet, M. A., Pather, S., and Dwyer, G.: Tracer experiment and model
809 evidence for macrofaunal shaping of microbial nitrogen functions along rocky shores,
810 Biogeosciences, 13, 3519-3531, doi:10.5194/bg-13-3519-2016, 2016.

811 Raimbault, P., and Garcia, N.: Evidence for efficient regenerated production and
812 dinitrogen fixation in nitrogen-deficient waters of the South Pacific Ocean: impact on
813 new and export production estimates, Biogeosciences, 5, 323-338, 2008.

814 Santoro, A., Sakamoto, C., Smith, J., Plant, J., Gehman, A., Worden, A., Johnson, K.,
815 Francis, C., and Casciotti, K.: Measurements of nitrite production in and around the
816 primary nitrite maximum in the central California Current, Biogeosciences, 10,
817 7395-7410, doi:10.5194/bg-10-7395-2013, 2013.

818 Santoro, A. E., Casciotti, K. L., and Francis, C. A.: Activity, abundance and diversity of
819 nitrifying archaea and bacteria in the central California Current, Environ. Microbiol.,
820 12, 1989-2006, doi. L., and Francis, C. A.: Activity, abundance and diversity of
821 nitrifying archaea and bacteria in the central California Current, Environ. Microbiol.,
822 12, 1989-2006, 2010.

823 Santoro, A. E., Dupont, C. L., Richter, R. A., Craig, M. T., Carini, P., Mcilvin, M. R.,
824 Yang, Y., Orsi, W. D., Moran, D. M., and Saito, M. A.: Genomic and proteomic
825 characterization of "Candidatus Nitrosopelagicus brevis": An ammonia-oxidizing
826 archaeon from the open ocean, Proceedings of the National Academy of Sciences of the
827 United States of America, 112, 1173-1178, doi: 10.1073/pnas.1416223112, 2015.

828 Sigman, D., Casciotti, K., Andreani, M., Barford, C., Galanter, M., and Böhlke, J.: A
829 bacterial method for the nitrogen isotopic analysis of nitrate in seawater and freshwater,
830 Anal. Chem., 73, 4145-4153, doi: 10.1021/ac010088e, 2001.

831 Smith, J. M., Chavez, F. P., and Francis, C. A.: Ammonium uptake by phytoplankton
832 regulates nitrification in the sunlit ocean, PloS One, 9, e108173, doi:
833 org/10.1371/journal.pone.0108173, 2014.

834 Sunda, W. G., and Ransom, H. D.: Ammonium uptake and growth limitation in marine
835 phytoplankton, Limnol. Oceanogr., 52, 2496–2506, 2007.

836 van Kessel, M. A., Speth, D. R., Albertsen, M., Nielsen, P. H., Opden Camp, H. J.,
837 Kartal, B., Jetten, M. S., and Lucker, S.: Complete nitrification by a single
838 microorganism, Nature, 528, 555-559, 10.1038/nature16459, doi:10.1038/nature16459,
839 2015.

840 Varela, M. M., Bode, A., Fernandez, E., Gonzalez, N., Kitidis, V., Varela, M., and
841 Woodward, E.: Nitrogen uptake and dissolved organic nitrogen release in planktonic
842 communities characterised by phytoplankton size–structure in the Central Atlantic
843 Ocean, Deep Sea Res. Part I Oceanogr. Res. Pap., 52, 1637-1661,
844 doi:10.1016/j.dsr.2005.03.005, 2005.

845 Veuger, B., Middelburg, J. J., Boschker, H. T. S., Nieuwenhuize, J., Rijswijk, P. V.,
846 Rochelle-Newall, E. J., and Navarro, N.: Microbial uptake of dissolved organic and
847 inorganic nitrogen in Randers Fjord, Estuarine Coastal and Shelf Science, 61, 507–515,
848 doi:10.1016/j.ecss.2004.06.014, 2004.

849 Wada, E., and Hatton, A.: Nitrite metabolism in the euphotic layer of the central North
850 Pacific Ocean, Limnol. Oceanogr., 16, 766-772, doi: 10.4319/lo.1971.16.5.0766 1971.

851 Ward, B. B.: Temporal variability in nitrification rates and related biogeochemical
852 factors in Monterey Bay, California, USA, Mar. Ecol. Prog. Ser., 292, 109,
853 doi:10.3354/meps292097, 2005.

Ward, B. B.: Nitrification in marine systems, in Nitrogen in the marine environment, edited by: Capone, D. A., Bronk, D. A., Mulholland, M. R., Carpenter, E. J., Academic Press, London, U.K., 5, 199-261, 2008.

Ward, B. B.: Measurement and distribution of nitrification rates in the oceans, in Methods in enzymology, edited by Abelson, J. N., Simon, M. I., Academic Press, London, U.K., 486, 307-323, 2011.

Yool, A., Martin, A. P., Fernández, C., and Clark, D. R.: The significance of nitrification for oceanic new production, Nature, 447, 999-1002, doi:10.1038/nature05885, 2007.

Zehr, J. P., and Kudela, R. M.: Nitrogen cycle of the open ocean: from genes to ecosystems, Ann. Rev. Mar. Sci., 3, 197-225, doi: 10.1146/annurev-marine-120709-142819, 2011.

Zhang, L., Altabet, M. A., Wu, T., and Hadas, O.: Sensitive measurement of NH_4^+ $^{15}N/^{14}N$ ($\delta^{15}NH_4^+$) at natural abundance levels in fresh and saltwaters, Anal. Chem., 79, 5297-5303, doi: 10.1021/ac070106d, 2007.

Zhu, Y., Yuan, D., Huang, Y., Ma, J., and Feng, S.: A sensitive flow-batch system for on board determination of ultra-trace ammonium in seawater: Method development and shipboard application, Anal. Chim. Acta., 794, 47-54, 10.1016/j.aca.2013.08.009, doi:10.1016/j.aca.2013.08.009, 2013.

Table 1. The isotope matrix results for (A) the specific rates and (B) average rates of N processes in the low-nutrient case during the first interval under different r_{NH4+} variation conditions. And all N transformation rates via ODE following Pfister et al. (2016) on the assumption of no remineralization were estimated for comparison. Note r_{NH4+} variation was manipulated artificially by decreasing r_{NH4+} values at a constant reduction rate and the total reduction of rNH4+ was 0%, 1%, 10%, 20% and 50% of the full time span (24 h) of incubation.

(A)

Rate constant (k) h^{-1}	The percentage of r_{NH4+} decrease in 24 h					
	0		1%	10%	20%	50%
	ODE	Isotope Matrix				
NH_4^+ uptake (k1)	0.040	0.038	0.038	0.038	0.038	0.039
Remineralization (k2)	0	0	0.00001	0.0001	0.0002	0.001
NH_4^+ oxidation (k3)	0.0004	0.0005	0.0005	0.0005	0.0005	0.0005
NO_x^- uptake (k4)	0.060	0.059	0.059	0.059	0.059	0.059
DON release (k5)	0.017	0.024	0.024	0.024	0.024	0.024
Bacteria uptake NH_4^+ (k6)	0.005	0.007	0.008	0.011	0.015	0.028

(B)

Rate ($k \times$ C) nmol L^{-1} h^{-1}	The percentage of r_{NH4+} decrease in 24 h					
	0		1%	10%	20%	50%
	ODE	Isotope Matrix				
NH_4^+ uptake (F1)	3.8	4.9	4.9	4.9	5.0	5.1
Remineralization (F2)	0.0	0.0	0.1	0.6	1.2	3.0
NH_4^+ oxidation (F3)	0.04	0.07	0.1	0.1	0.1	0.7
NO_x^- uptake (F4)	19.3	27.2	27.2	27.2	27.2	27.2
DON release (F5)	9.6	11.5	11.5	11.6	11.6	11.8
Bacteria uptake NH_4^+ (F6)	0.5	1.0	1.0	1.5	2.0	3.7

Table 2. The isotope matrix results for the rates of N processes in the high-nutrient case at the depth of (A) 80% sPAR and (B) 2% sPAR under different r_{NH4+} variation conditions. And all N transformation rates via ODE following Pfister et al. (2016) on the assumption of no remineralization were estimated for comparison. Note: r_{NH4+} variation was manipulated artificially by decreasing r_{NH4+} values at a constant reduction rate and the total reduction of r_{NH4+} was 0%, 1%, 10%, 20% and 50% of the full time span (15 h) of incubation.

(A)

Rate (k* C) nmol L^{-1} h^{-1}	The percentage of r_{NH4+} decrease in 15 h					
	0		1%	10%	20%	50%
	ODE	Isotope Matrix				
NH_4^+ uptake (F1)	360	397	397	399	401	408
Remineralization (F2)	0	0	21	211	424	1043
NO_2^- uptake (F3)	27	29	29	29	29	29
NH_4^+ oxidation (F4)	1.1	0.4	0.4	0.4	0.4	0.4
NO_3^- uptake (F5)	190	149	149	149	149	149
NO_2^- oxidation (F6)	1.7	0	0	0	0	0
DON release (F7)	0	0	0	0	0	0
Bacteria uptake NH_4^+ (F8)	268	282	303	490	701	1314

(B)

Rate (k* C) nmol L^{-1} h^{-1}	The percentage of r_{NH4+} decrease in 15 h					
	0		1%	10%	20%	50%
	ODE	Isotope Matrix				
NH_4^+ uptake (F1)	228	208	208	209	211	216
Remineralization (F2)	0	0	18.1	179	361	895
NO_2^- uptake (F3)	7.3	3.1	3.1	3.1	3.1	3.1
NH_4^+ oxidation (F4)	1.1	0.7	0.7	0.7	0.7	0.7
NO_3^- uptake (F5)	106	72	72	72	72	72
NO_2^- oxidation (F6)	2.0	0	0	0	0	0
DON release (F7)	0	0	0	0	0	0
Bacteria uptake NH_4^+ (F8)	202	265	283	442	623	1152

892 **Table 3.** Comparison of the NH_4^+/ NO_x^- uptake and NH_4^+ oxidation/nitrification rates

893 derived from different methods.

Process	Case	Depth (m)	Isotope Matrix method (this study)	Rates based on Ref A*	Traditional method Ref B*	Rates followed Ref C*
			(nmol L^{-1} h^{-1})			
NH_4^+ uptake	Low nutrient	25	4.9	3.8	4.6	
Nitrification	Low nutrient	25	0.07	0.04	−	0.05
NO_x^- uptake	Low nutrient	25	27.2	19.3		4.6
NH_4^+ uptake	High -80%sPAR	0.2	397	360	387	
NH_4^+ oxidation	High -80%sPAR	0.2	0.4	1	−	
NH_4^+ uptake	High -2% sPAR	2.3	208	228	192	
NH_4^+ oxidation	High -2% sPAR	2.3	0.7	1	−	

894 Ref A* stands of rates calculation by ODE followed Pfister et al. (2016)

895 Ref B* stands of rates calculation followed Collos (1987)

896 Ref C* stands of rates calculation followed Santoro et al. (2010)

897

898 **Table 4.** The contribution of nitrification derived NO_x^- to NO_x^- uptake (%), N
899 preference index, and the proportion of NH_4^+ consumption by phytoplankton, bacteria
900 and nitrifier to total NH_4^+ consumption in low and high nutrient cases.

Case	Depth (m)	nitrification to NO_3^- uptake (%)	RPI for NH_4^+	RPI for NO_2^-	RPI for NO_3^-	*A/TNH_4^+ consumption (%)	*B/TNH_4^+ consumption (%)	*C/TNH_4^+ consumption (%)
Low nutrient	25	0.3	0.9		1.0	82.1	16.8	1.2
High -80%sPAR	0.2	0.3	1.6	0.6	0.5	58.4	41.5	0.1
High -2% sPAR	2.3	0.9	1.8	0.1	0.5	43.9	56.0	0.1

901 *A, *B, *C stands for NH_4^+ utilized by phytoplankton, bacteria and nitrifier,
902 respectively. TNH_4^+ consumption stands for total NH_4^+ consumption.

903

Figure Captions

Fig. 1. Model schemes with the most fundmental nitrogen transformation processes in low- (a) and high- (b) nutrient aquatic environments. Arrows stand for the transfer flux/rate from the reactant to product pool. The structure and inter-exchanges in the high-nutrient case (Fig. 1b) are the same as in (a), except that NO_x^- is divided into NO_2^- and NO_3^-.

Fig. 2. The observational data in the low-nutrient case for (a) $[NH_4^+]$, (b) $[NO_x^-]$, (c) [PN], (d) [TDN], (e) $\delta^{15}N\text{-}NO_x^-$, (f) $\delta^{15}N$-PN. The regular and inverse open triangles stand for the paralled samples and the analytical errors are shown.

Fig. 3. The observational data in the high-nutrient case for (a) $[NH_4^+]$, (b) $[NO_2^-]$, (c) $[NO_3^-]$, (d) [PN], (e) [TDN], (f) [PN+TDN], (g) $\delta^{15}N\text{-}NO_2^-$, (h) $\delta^{15}N\text{-}NO_3^-$ and (i) $\delta^{15}N$-PN. The light and dark red diamonds stand for the paralled samples in 80% sPAR case and the black regular and inverse open triangles stand for the paralled samples in 2% sPAR case. The analytical errors are shown in figures.

Fig. 4. The observed and STELLA-derived values in the low-nutrient case for (a) $[^{15}NH_4^+]$, (b) $[^{15}NO_x^-]$, (c) [^{15}N-PN], (d) [^{15}N-DON], (e) $[^{14}NH_4^+]$, (f) $[^{14}NO_x^-]$, (g) [^{14}N-PN], (h) [^{14}N-DON], (i) r_{NH4+}, (j) r_{NOx-}, (k) r_{PN}, (l) r_{DON}, (m) $\delta^{15}N\text{-}NH_4^+$, (n) $\delta^{15}N\text{-}NO_x^-$, (o) δ^{15}N-PN, (p) δ^{15}N-DON, (q) $[NH_4^+]$, (r) $[NO_x^-]$, (s) [PN] and (t) [DON]. The black regular and inverse open triangles represent the paralleled observed values; the black, green, blue, magenta and pink solid lines stand for the STELLA model simulations when r_{NH4+} decreases 0%, 1%, 10%, 20% and 50% in 24 h, respectively. The dashed lines in (b), (f), (j), (n) and (r) were generated from nonlinear least-squares curve-fitting by Matlab following Santoro et al. (2010).

Fig. 5. The observed and STELLA-derived values in the high-nutrient case of (A) 80% sPAR depth and (B) 2% sPAR depth for (a) $[^{15}NH_4^+]$, (b) $[^{15}NO_2^-]$, (c) $[^{15}NO_3^-]$, (d) [^{15}N-PN], (e) [^{15}N-DON], (f) $[^{14}NH_4^+]$, (g) $[^{14}NO_2^-]$, (h) $[^{14}NO_3^-]$, (i) [^{14}N-PN], (j)

930 [^{14}N-DON], (k) r_{NH4+}, (l) r_{NO2-}, (m) r_{NO3-}, (n) r_{PN}, (o) r_{DON}, (p) δ^{15}N-NH_4^+, (q)
931 δ^{15}N-NO_2^-, (r) δ^{15}N-NO_3^-, (s) δ^{15}N-PN, (t) δ^{15}N-DON, (u) [NH_4^+], (v) [NO_2^-], (w)
932 [NO_3^-] (x) [PN] and (y) [DON]. The black regular and inverse open triangles
933 represent the duplicate observational values; the black, green, blue, magenta and pink
934 solid lines represent the STELLA model simulations of r_{NH4+} decreases 0%, 1%, 10%,
935 20% and 50% in 15 h, respectively.
936

937 **Fig. 1**

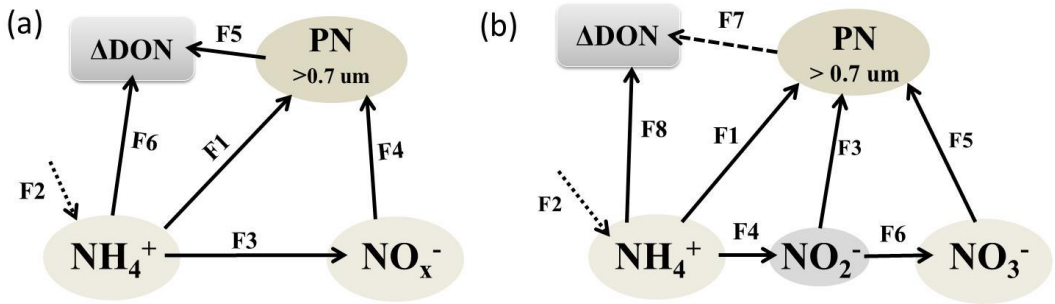

938

939

940 **Fig. 2**

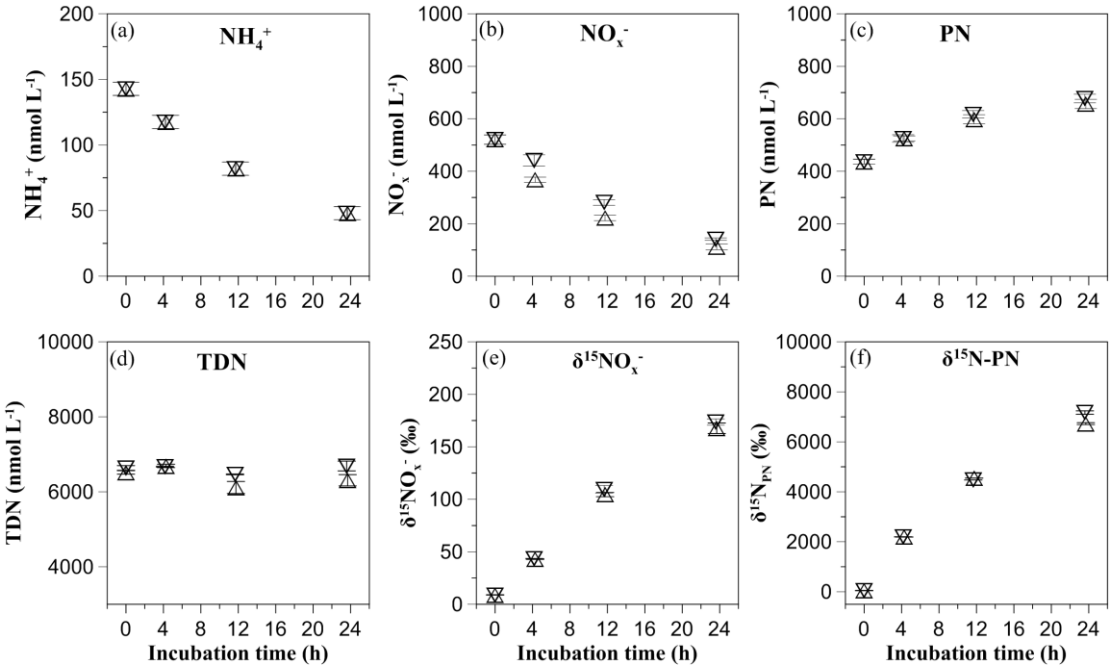

941

942

943 **Fig. 3**

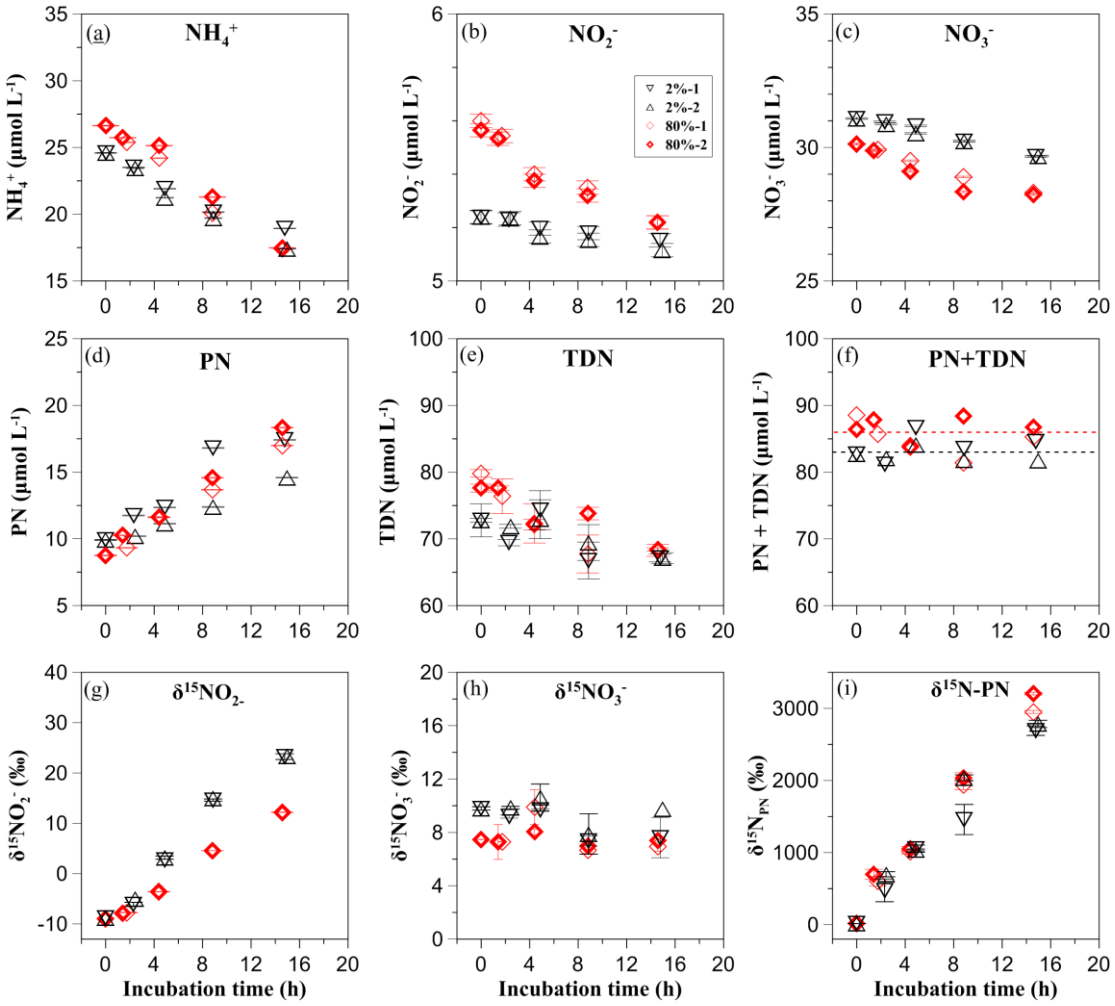

944

945

946 **Fig. 4**

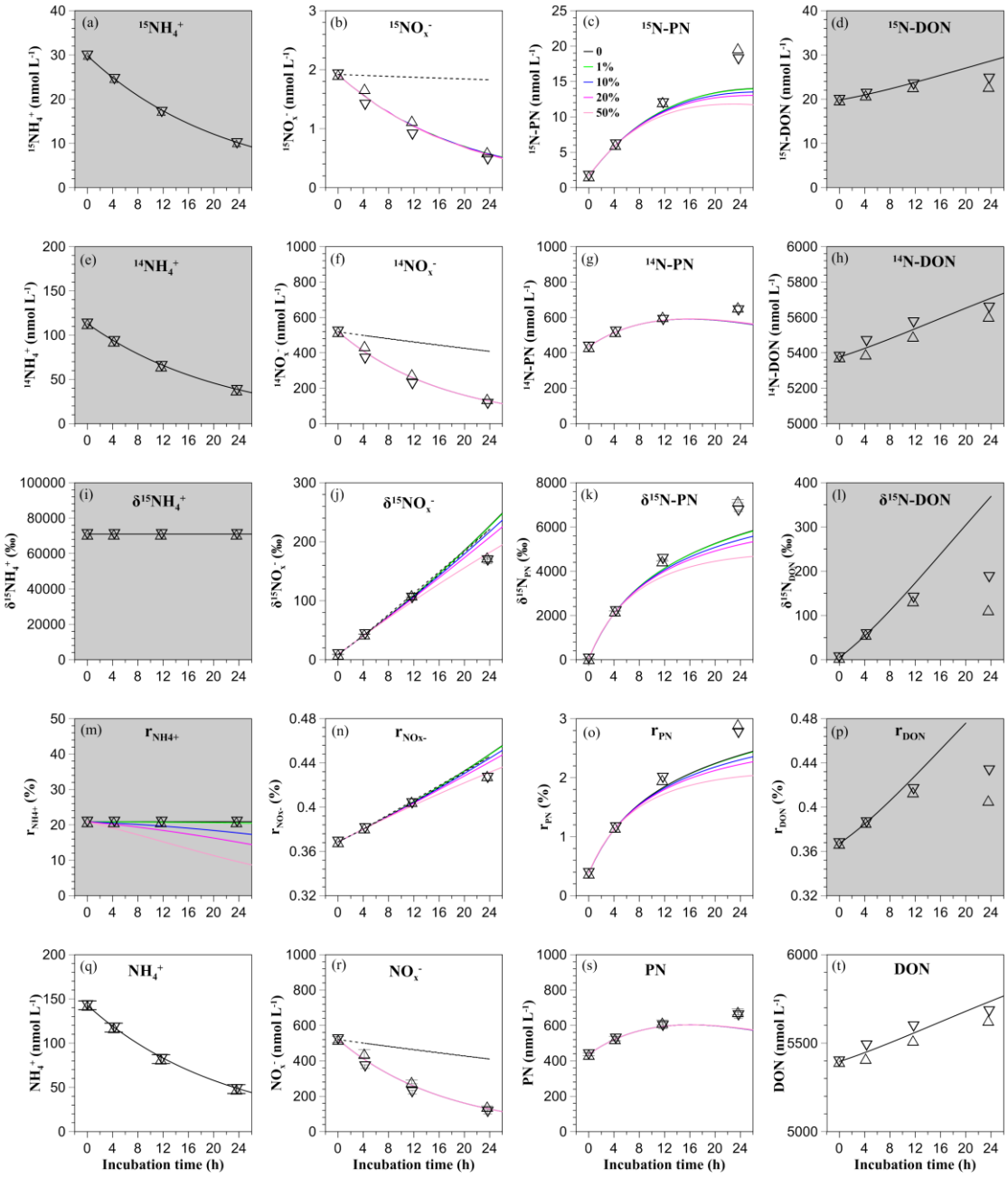

947

948

Fig. 5(A)

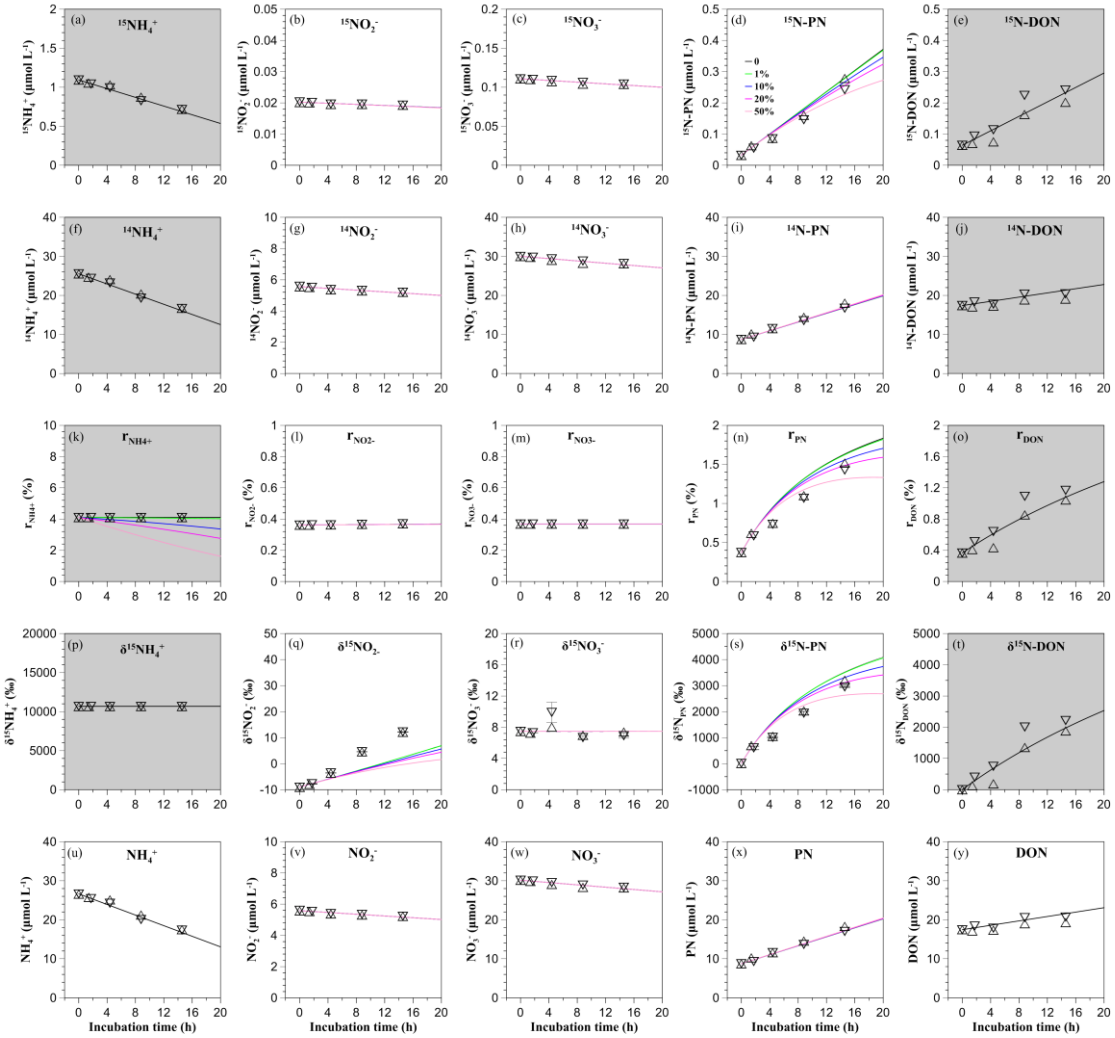
(a) $^{15}NH_4^+$
(b) $^{15}NO_2^-$
(c) $^{15}NO_3^-$
(d) ^{15}N-PN
(e) ^{15}N-DON
(f) $^{14}NH_4^+$
(g) $^{14}NO_2^-$
(h) $^{14}NO_3^-$
(i) ^{14}N-PN
(j) ^{14}N-DON
(k) r_{NH4+}
(l) r_{NO2-}
(m) r_{NO3-}
(n) r_{PN}
(o) r_{DON}
(p) $\delta^{15}NH_4^+$
(q) $\delta^{15}NO_2^-$
(r) $\delta^{15}NO_3^-$
(s) $\delta^{15}N$-PN
(t) $\delta^{15}N$-DON
(u) NH_4^+
(v) NO_2^-
(w) NO_3^-
(x) PN
(y) DON
0
1%
10%
20%
50%
Incubation time (h)

952 **Fig. 5(B)**

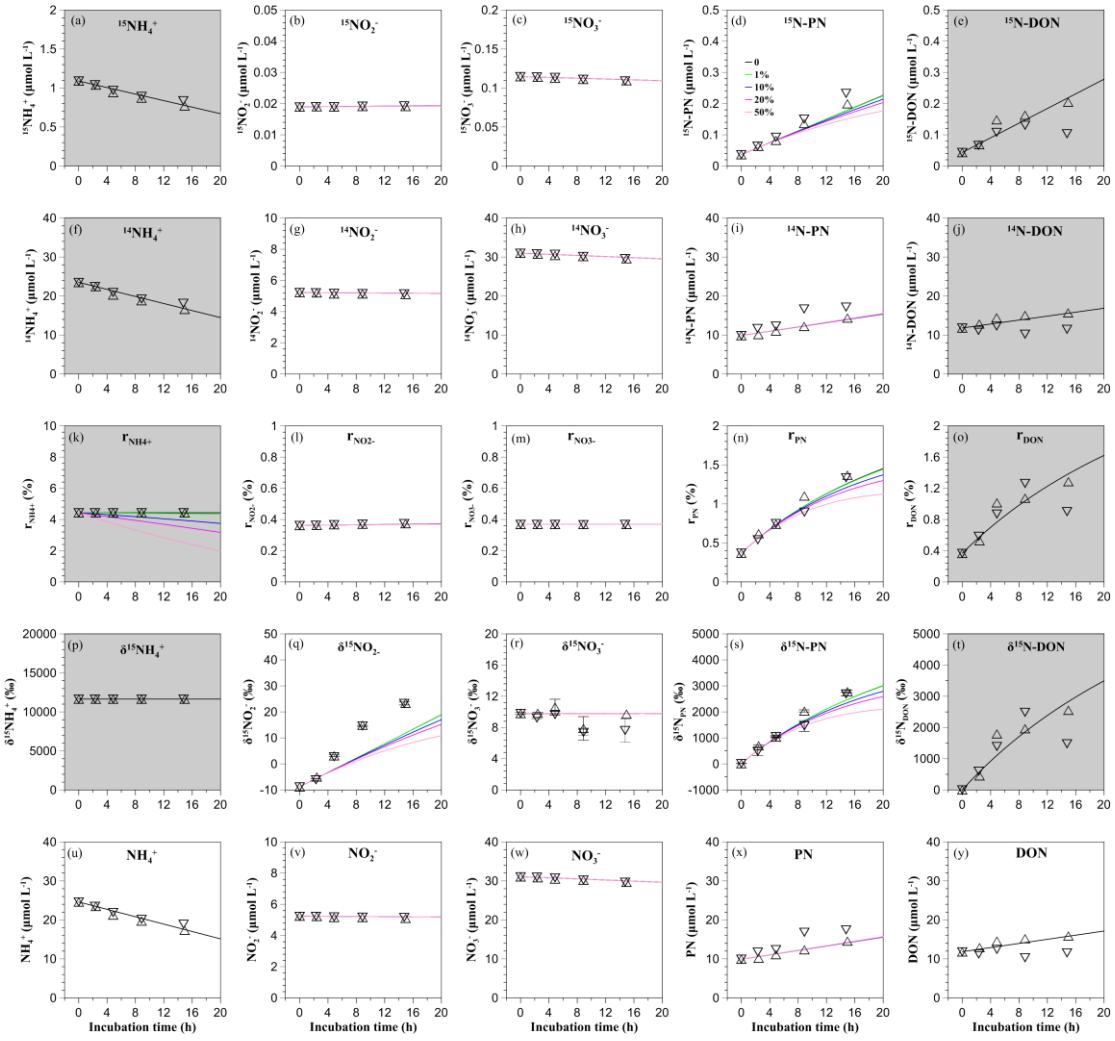

953